for a Sustainable Environment (eds Doran, J. W and Parking, T. B.), Special Publication No. 35. Soil Science Society of America, Madison, WI, 1994, pp. 53–72.
36. Sys, C., *Land Evaluation: Part I*, University of Ghent, Ghent, 1985.
37. Andrews, S. S., Karlen, D. L. and Mitchell, J. P. A., Comparison of soil quality indexing methods for vegetable production systems in northern California. *Agric. Ecosyst. Environ.*, 2002, **90**, 25–45.
38. Lal, R., *Methods and Guidelines for Assessing Sustainable Use of Soil and Water Resources in the Tropics*, Scientific Publishers, Jodhpur, 1996.
39. Tiessen, H., Cuevas, E. and Chacon, P., The role of organic matter in sustaining soil fertility. *Nature*, 1994, **371**, 783–785.
40. Grossman, R. B., Harms, D. S., Seybold, C. A. and Herrick, J. E., Coupling use-dependent and use-invariant data for soil quality evaluation in the United States. *J. Soil Water Conserv*., 2001, **56**, 63–68.
41. Singh, R., Shrimali, S. S. and Sharma, N. K., Soil surface management for erosion control, CSWCRTI Annual Report (2003–2004), Dehradun, 2004.
42. Nalatwadmath, S. K., Patil, S. L., Adhikari, R. N. and Reddy, K. K., Erosion productivity relationship for evaluating vulnerability and resilience of soils under different agro-ecological regions. CSWCRTI Annual Report (2009–2020), Dehradun, 2010.
43. Singh, K. D., Participatory watershed management – a key to sustainable agriculture. *J. Indian Soc. Soil Sci*., 2006, **54**, 443–451.
44. Larson, W. E. and Piece, F. J., Conservation and enhancement of soil quality. In *Evaluation for Sustainable Land Management in the Developing World* (eds Dumanski, J. *et al.*), Proceedings of International Workshop, Technical Papers, International Board for Soil Research and Management, Bangkok, Thailand, 1991, vol. 2, pp. 175–203.
45. Doran, J. W. and Parkin, T. B., Defining and assessing soil quality. In *Defining Soil Quality for a Sustainable Environment* (eds Doran, J. W. *et al.*), Special Publication No. 35, Soil Science Society of America, Madison, Wisconsin, 1994, pp. 3–21.
46. Arshad, M. A., Lowery, B. and Grossman, R. B., Physical tests for monitoring soil quality. In *Methods of Assessing Soil Quality* (eds Doran, J. W. and Jones, A. J.), Special Publication No. 49, Soil Science Society of America, Madison, Wisconsin, 1996, pp. 123–141.
47. Harris, R. F., Karlen, D. L. and Mulla, D. J., A conceptual framework for assessment and management of soil quality and health. In *Methods for Assessing Soil Quality* (eds Doran, J. W. and Jones, A. J.), Special Publication No. 49, Soil Science Society of America, Madison, Wisconsin, 1996, pp. 61–82.
48. Karlen, D. L., Parkin, T. B. and Eash, N. S., Use of soil quality indicators to evaluate conservation reserve program sites in Iowa. In *Methods for Assessing Soil Quality* (eds Doran, J. W. and Jones, A. J.), Special Publication No. 49, Soil Science Society of America, Madison, Wisconsin, 1996, pp. 345–356.

ACKNOWLEDGEMENTS. We thank the scientists of Central Soil and Water Conservation Research and Training Institute (CSWCRTI), Dehradun who have directly or indirectly contributed to ensure timely completion of the study. Financial support provided by the institute to undertake this study is also acknowledged.

Received 12 February 2010; revised accepted 11 November 2010

Effect of Himalayan topography on two-dimensional interpretation of magnetotelluric data

G. Pavan Kumar* and A. Manglik

National Geophysical Research Institute (CSIR), Uppal Road, Hyderabad 500 606, India

Magnetotelluric method is a powerful tool for deep crustal studies of tectonically active mountainous regions such as the Himalaya, where logistic constraints severely limit the use of other artificial source electrical and electromagnetic methods. Topographic variations in mountainous regions distort apparent resistivity curves and thus lead to artefacts in interpreted models. In the present work, we have analysed a simplified two-dimensional (2D) model of the subsurface electrical resistivity structure along a profile in the Garhwal Himalaya for the effect of topography. The topography varies significantly along the profile between the foothills and the higher Himalaya. We first computed TE and TM-mode apparent resistivity and phase curves at various stations along the profile for a model with topography and then inverted these datasets for two cases. In the first case the surface of the earth was assumed to be flat, whereas in the second case the actual topography was included in the model. The results suggest that the interpreted model assuming flat earth is similar to the one obtained by including topography in the model. Inclusion of 10% Gaussian noise to the synthetic data does not change these results. Thus, we infer that the effect of 2D topography is not prominent in the 2D interpretation of the selected Garhwal Himalaya profile.

Keywords: Magnetotelluric data, mountainous regions, resistivity curves, topographic variations.

MAGNETOTELLURIC (MT) method is a powerful tool for the delineation of deep crustal structure because electromagnetic (EM) signals penetrate deeper into the earth as the frequency of the signal decreases. Natural EM sources contain a broad range of frequencies, making it possible to scan the crustal structure at various depths and resolutions. The usefulness of the method becomes pronounced in tectonically active mountainous regions, such as the Himalaya, where logistic constraints severely limit the use of other artificial source electrical and EM methods for deep crustal studies. The topographic variations of mountainous regions distort the resistivity curves for recording sites in the vicinity of a topographic feature[1–3]. Inversion of these distorted curves due to the effect of topography yields spurious structural features.

*For correspondence. (e-mail: gayatripavan@ngri.res.in)

Telluric currents flow parallel to the surface. In areas with topography, their geometry is distorted showing convergence in valleys and divergence in hilltop regions leading to an increase in the electric field and hence the apparent resistivity under the valleys, and a decrease in the electric field and apparent resistivity beneath the hills[2,4]. For two-dimensional (2D) topography the E-field across the topography is most distorted, whereas the one parallel to the strike of topography is least affected. Thus, the TM-mode data show pronounced effect of topography[5] compared to the TE-mode in which the perturbations are small and quickly vanish, when the typical scale length of topographic features is small compared to the skin depth in the subsurface[6]. However, three-dimensional (3D) topography variations lead to a more complex pattern of distortion. For a 2D topography, the effect is galvanic in the TM-mode and inductive in the TE-mode[7], whereas for a 3D topography both effects dominate in all modes[8].

The effects of 2D topography on MT data have been extensively studied mostly by numerical modelling approach[9–12]. Some analytical solutions have also been obtained using Schwarz Christoffel transformations[13,14]. In recent years, numerical modelling studies have been carried out to analyse the effect of 3D topography[8,15]. Several studies have been carried out to interpret MT data affected by topography distortions following two approaches. The first approach is focused on estimation of distortion tensor and correction of MT data before inversion[16–18]. In the second approach, the topography is explicitly included in the model. Here, numerical codes based on finite element method[5,19] have an advantage over finite difference codes[20,21] as these are able to include irregular surfaces. Aprea *et al.*[22] and Li *et al.*[12] included special treatment of resistivity at surface nodes to improve finite difference solutions.

In the present work, we have considered a profile across the Himalaya and analysed the effect of topography on the 2D interpretation of MT data. The topography varies significantly along the profile between the foothills and the higher Himalaya. We have analysed a simplified model of the interpreted subsurface electrical resistivity structure along the Garhwal Himalaya profile[23] by first computing TE and TM-mode apparent resistivity and phase curves, including topography at various stations and then inverting these datasets assuming models with flat earth and with topography. We have also analysed the effect of noise in the data on the inversion results.

The Himalaya extends for more than 2500 km from west to east. Despite such a long and complex tectonic set-up, only a limited number of MT profiles have been covered across it to obtain the electrical resistivity structure. Gokarn *et al.*[24] delineated the crustal electrical resistivity structure of Zhanskar range, Tso Morari dome and Ladakh batholith in NW Himalaya. Arora *et al.*[25] acquired long-period MT data and interpreted the deeper structure along the same profile and inferred the presence of partial melt beneath the Indus Tsangpo Suture Zone and Ladakh. Israil *et al.*[23] studied a profile in the Garhwal Himalaya and found a correlation between the seismicity in this region with a high conductivity zone beneath the Main Central Thrust (MCT). Lemonnier *et al.*[26] covered a profile across the central Himalaya and correlated the high conductivity zone beneath the front of the Higher Himalaya with the presence of metamorphic fluids. These studies also bring out the dip of the Indian plate as it underthrusts beneath the Himalaya. In the eastern segment, Patro and Harinarayana[27] have delineated the resistivity structure beneath the Sikkim Himalaya, and Gokarn *et al.*[28] analysed a profile covering the Shillong plateau and the Brahmaputra valley. Besides, there are many MT studies covering the Higher Himalaya and Tibet.

We have taken the Garhwal Himalaya profile[23] to analyse the effect of topography. The topography increases from about 100 m at the foothills of the Himalaya to more than 3 km at the Higher Himalaya within a lateral distance of about 160 km. A simplified profile of the topography is shown in Figure 1 *a*. We further simplify the subsurface resistivity model of Israil *et al.*[23], shown in Figure 1 *b*, to keep only major features in the model as our objective is to analyse the effect of topographic variations. In the simplified model, the Indian plate gently dips northward in the southern segment of the profile, forms a ramp structure with associated high conductivity zone at MCT, and then flattens further north. Thus, the whole model is subdivided into four major zones.

This model along with the topography is used to compute forward TE and TM-mode apparent resistivities and phase responses at 16 sites along the profile using a 2D smooth inversion code[29] implemented in a commercial package WinGlink (M/s. Geosystems). TE-mode represents the resistivity structure along the geological strike direction (and TM along the orthogonal direction) for a

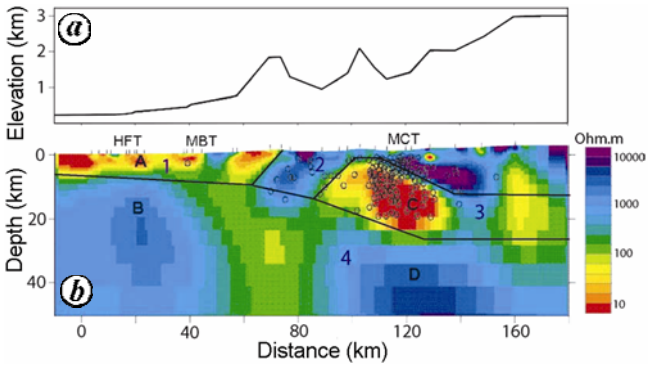

Figure 1. Topography (***a***) and 2D crustal electrical resistivity structure (***b***) along a profile in the Garhwal Himalaya (modified after Israil *et al.*[23]). Simplified crustal model (solid black lines) used in the present work is superimposed and four zones (1–4) have the resistivity of 25, 5000, 10 and 1000 Ohm.m respectively. HFT, Himalayan Frontal Thrust; MBT, Main Boundary Thrust, and MCT, Main Central Thrust. A, B, C, D indicate the major geoelectrical features of the model.

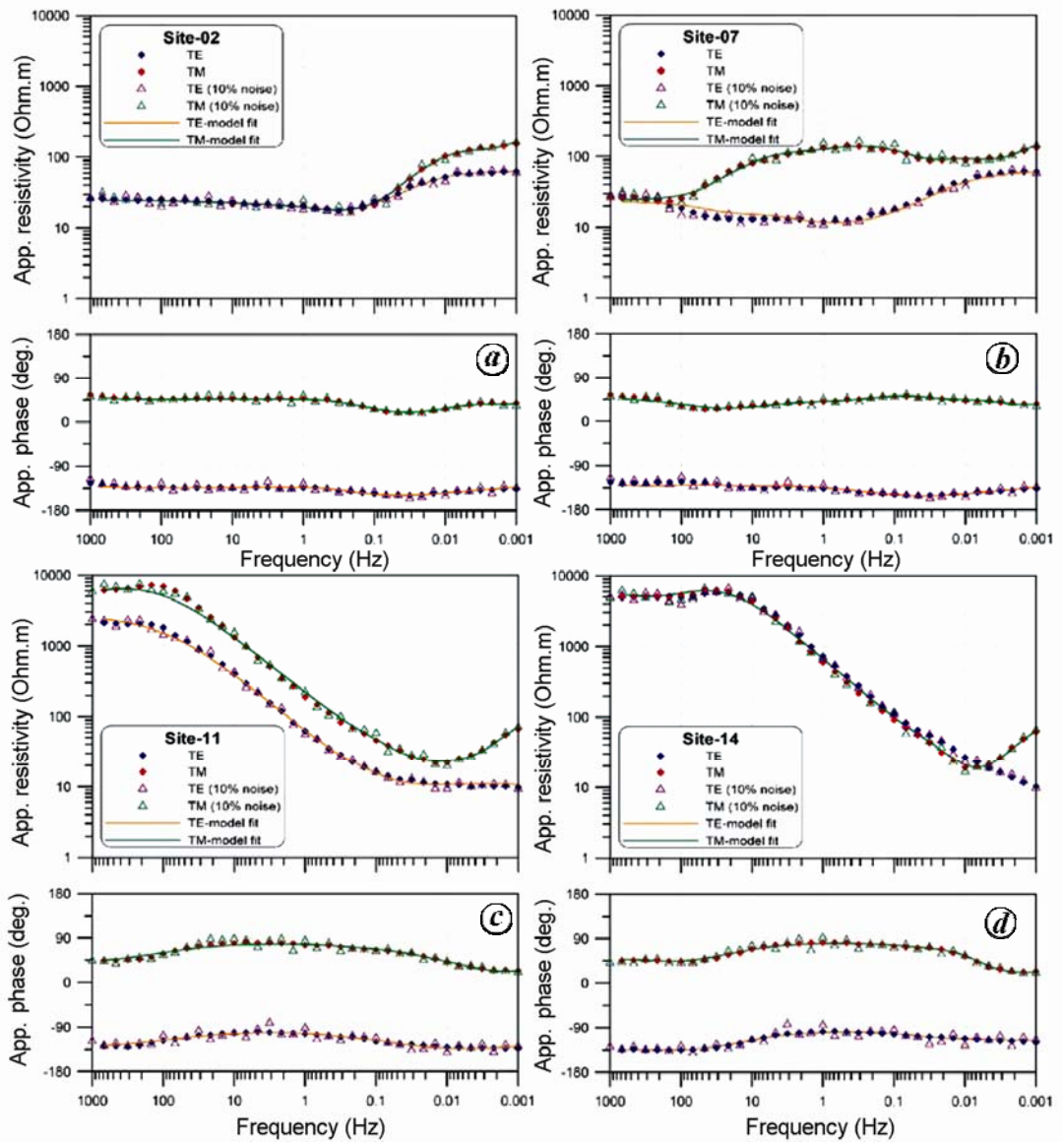

Figure 2. Synthetic apparent resistivity and phase response at four sites for the simplified crustal model with topography shown in Figure 1. Filled and open symbols represent noise-free and noisy (with 10% Gaussian distribution) data respectively. These data have been used as observed responses for the flat earth and topography models. Solid curves show the response of the best-fit model for the noisy data. Locations of the sites are marked in Figure 3.

2D structure and in many practical situations this may not coincide with the profile direction. However, for the present study we assume that the geological strike is perpendicular to the profile direction as the general geological strike of N70W in this region obtained by Israil *et al.*[23] is nearly orthogonal to the profile direction. Therefore, in the present study TE-mode is orthogonal to the profile direction.

Synthetic responses at some sites are shown in Figure 2 (filled symbols). In the southern segment (site-2) where the Indian plate gently dips, the TE and TM-mode apparent resistivities are almost the same up to 10 s period, beyond which they split. The TE and TM-mode curves show different patterns at sites covering the regions consisting of lateral heterogeneities and ramp structure (e.g. sites 7 and 11; Figure 2). The structure is again uniform further north (site-14) with a resistive layer of 5000 Ohm.m resistivity overlying a conducting zone of 10 Ohm.m resistivity. We have also included Gaussian noise to these responses to generate synthetic noisy data. Two different datasets were generated by adding noise with 5% and 10% standard deviation respectively, to the mean values of the apparent resistivity and phase. The datasets corresponding to 10% noise are shown in Figure 2 (open symbols).

We have inverted the above noise-free synthetic responses for two different scenarios. In the first scenario, we assumed a flat earth model and in the second we

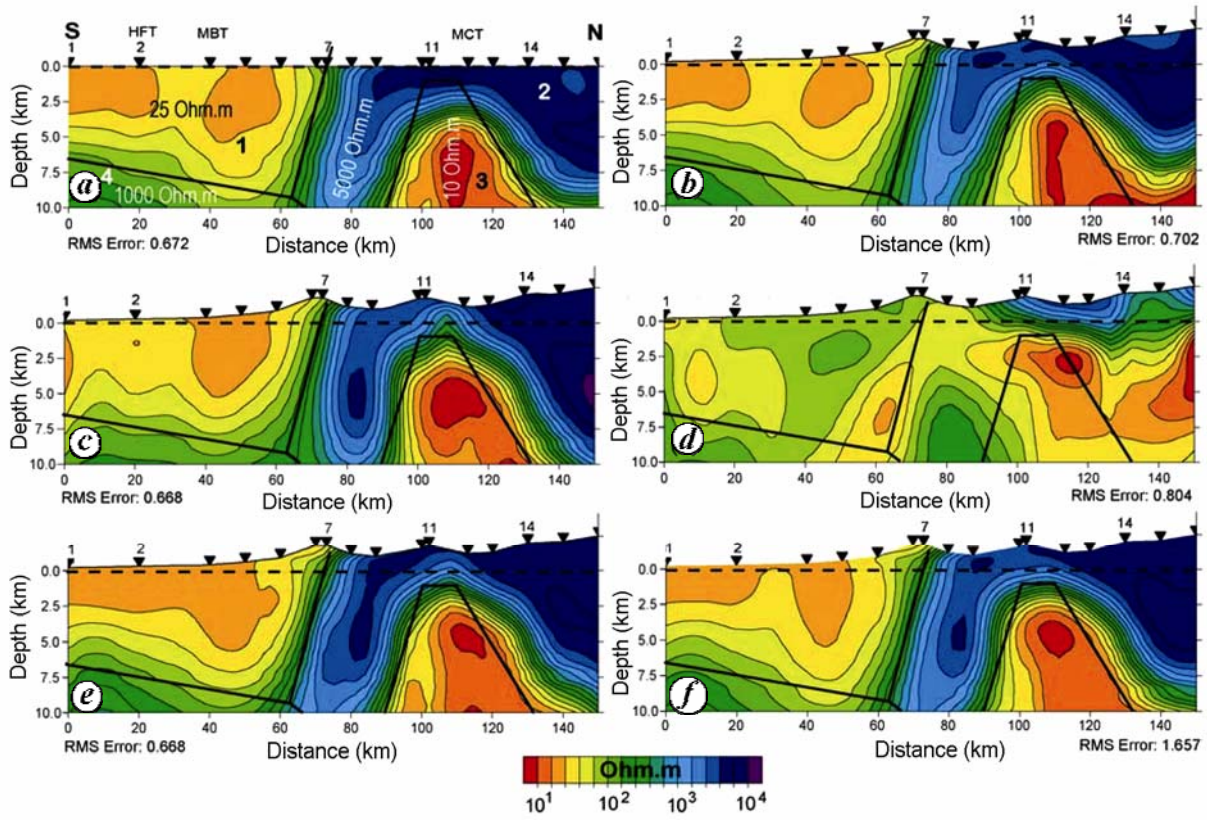

Figure 3. Various models of 2D crustal structure after inversion of synthetic apparent resistivity and phase response. ***a***, Flat earth model (model 1) after joint inversion (JI) of TE and TM-mode data; ***b***, Model with topography (model 2) after JI starting with inversion of TM-mode; ***c***, Model 2 after TM-mode inversion; ***d***, Model 2 after TE-mode inversion; ***e***, Model 2 after JI starting with inversion of TE-mode, and ***f***, Same as (***e***) but for data corrupted with 10% Gaussian noise. Solid thick black lines represent true model. Resistivity values of the true block model are also mentioned in (***a***).

included topography in the model. The data were inverted using WinGlink software. The initial model for both cases consisted of a homogeneous half-space of 100 Ohm.m resistivity. As the TM-mode is sensitive to lateral heterogeneities and the present model consists of steeply dipping contacts, we first inverted only TM-mode data. The inverted model thus obtained was used as an initial guess for the TE-mode data. Finally, the model obtained after the inversion of TE-mode data was used to jointly invert TE and TM-mode data.

The final models corresponding to the flat earth (model 1) and topography (model 2) are shown in Figure 3 *a* and *b* respectively. The results are shown only up to 10 km depth to highlight any changes in the model results at shallow depths. The results indicate that the major features of the model are reproduced for both cases, although there are minor changes near the topographic feature. For example, the near-surface resistivity at sites 6 and 7 and between sites 9 and 11 is lower in the model with topography compared to the flat earth model. Major differences are observed in the northern segment of the profile. The top resistive layer seems to be thinned by about 70% in the model with topography compared to the flat earth model in the region between sites 11 and 12. Similarly, the thickness of the resistive block beneath site 15 is also less and the deeper conducting layer is seen at relatively shallow depth.

It is to be noted that additional material is present between the mean sea level (zero depth, marked by dashed line) and the topographic surface in the model with topography. Therefore, the above differences could be an artifact arising due to the shifting of the layers upward in the presence of topography. We analyse this by plotting depth sections beneath sites 12 and 15 for both models. These results are shown in Figure 4. Here the zero depth is kept at the surface of topography instead of at the mean sea level. Thus, the depth section corresponding to the model with topography (solid curve) is shifted downward by an amount equal to the topographic height at the site. The true model is also shown by thick solid line. The results reveal that the depth sections for models with and without topography are almost the same. Thus, we infer that the topography effect does not seem to be prominent along the selected Garhwal Himalaya profile.

We further analyse the resolvability of resistivity and thickness of various blocks in the synthetic model by individual TE-mode and TM-mode inversion of synthetic noise-free data. For these inversions, we start with the same

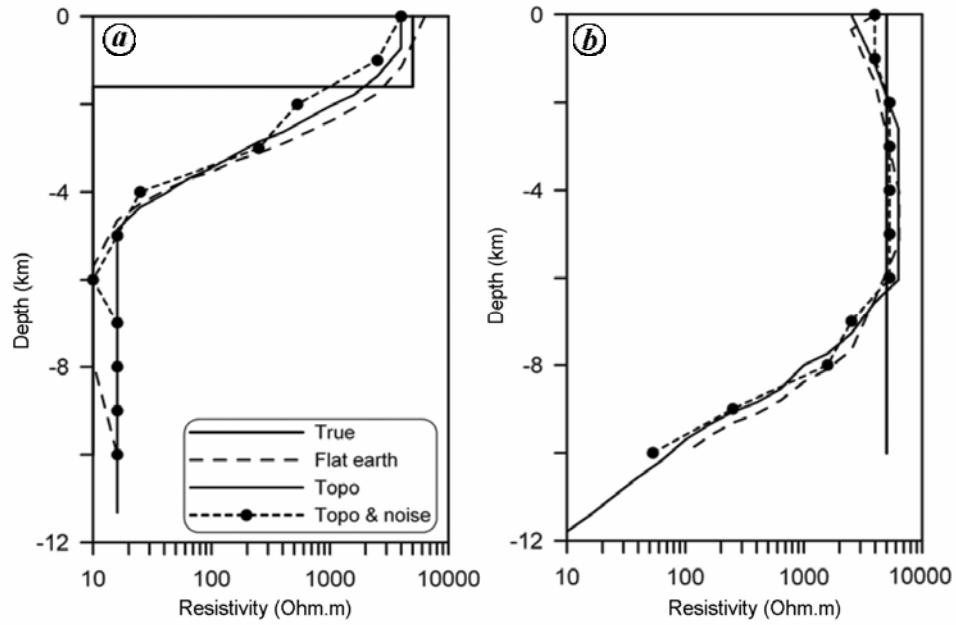

Figure 4. Variation of resistivity with depth at (***a***) site-12 and (***b***) site-15 after inversion of noise-free data assuming flat earth model (dashed curve) and topography model (solid curve). The results after inversion of noisy data with 10% Gaussian noise for topography model are shown by dashed curve with solid circles. Thick solid line represents the true model ('True'). Thin solid curve represents the inverted model including topography ('Topo').

initial model as used in previous computations. The model after inversion of TM-mode data (Figure 3 *c*) reveals major features of the original model consisting of nearly vertical blocks in the central and northern part of the profile, highlighting the advantage of using TM-mode data in resolving lateral heterogeneities. The model obtained after inversion of TE-mode data (Figure 3 *d*) is not able to resolve these block structures. Instead, the result shows a tendency of the TE-mode to resolve layered structure. This leads to distortion of the structure and the resistivity of various vertical blocks.

It is also interesting to analyse whether the sequence of TE and TM inversions has a pronounced effect on the estimated model after joint inversion (JI). To check this, we have computed another model in which we started with inversion of TE-mode data and then used the derived model as an initial guess for the inversion of TM-mode data. The final model thus obtained was then used to perform JI and the result is shown in Figure 3 *e*. Comparing this model with the one shown in Figure 3 *b* reveals that while broad structural features remain the same, there are some prominent changes in the fine resistivity structure. For example, block-2 (5000 Ohm.m) seems to be less resistive and thinner in Figure 3 *b* compared to that in Figure 3 *e*. Similarly, conductive block-3 is present at shallower depth beneath sites 14–16 in comparison to Figure 3 *e*. The resistivity of block-1 that extends laterally (sites 1–6) seems to be in good agreement between the two results. From these results it can be inferred that TE-mode inversion, if performed after TM-mode inversion, (sequence TM → TE → JI) tries to stretch the model in the lateral direction thus distorting the lateral heterogeneities, as seen in Figure 3 *b*. The opposite sequence of inversion (sequence TE → TM → JI) helps in the preservation of lateral heterogeneities, as seen in Figure 3 *e*. Thus, it would be useful to follow the sequence (TE → TM → JI) for models having vertical/steeping dipping contacts, e.g. in the Himalaya, whereas the sequence (TM → TE → JI) should be useful for the foreland Ganga basin.

Actual field data normally contain noise, which can arise due to various reasons such as cultural activities and geological complexities. In order to analyse the effect of noise on the inversion results, we have contaminated the synthetic data with Gaussian noise and then inverted these datasets following the same approach as discussed above. We analysed the models for 5% and 10% noise in the data and for both sequences of inversion (TM → TE → JI) and (TE → TM → JI). In Figure 3 *f*, we show one such result for 10% noise case as an extreme model. This model has been obtained by first inverting TE-mode data, then TM-mode data, and finally joint data. For this model, the RMS error after 90 iterations is about 2.5 times larger than the corresponding noise-free case (Figure 3 *e*) and there is no further improvement. The results, however, are largely similar to the corresponding noise-free case. Variation of resistivity with depth at sites 12 and 15 is also similar to the noise-free results (dashed curve with filled circles, Figure 4).

The above analysis employing a simplified model of the 2D crustal resistivity structure and topographic variations along a Garhwal Himalaya profile suggests that the

interpreted model, after inversion of joint TE and TM-mode data, assuming flat earth is similar to the one obtained by including topography in the model. In the present model, topography increases from about 100 m at the foothills of the Himalaya to more than 3 km in the Higher Himalaya within a lateral distance of about 160 km. Nevertheless, the broad features of the crustal structure are consistently reproduced in the flat earth case. Thus, we infer that the topography effect is not prominent along the selected Garhwal Himalaya profile. Inversion of TM-mode data is found to better constrain the vertical conductive and resistive structures seen in the central and northern part of the profile compared to the inversion of TE-mode data.

In the present analysis, we have assumed that the topography is 2D in nature as it does not vary in the direction orthogonal to the profile direction. However, the Himalayan topography is more complex and 3D in nature. Therefore, both inductive and galvanic effects might influence MT data and still yield spurious results. This may be analysed in future and would need MT data on a grid instead of those along a profile.

1. Schnegg, P. A., Le Quang, B. V., Fischer, G. and Weaver, J. T., Audio-magnetotelluric study of a structure with a reverse fault. *J. Geomagn. Geoelectr.*, 1983, **35**, 653–671.
2. Chouteau, M. and Bouchard, K., Two-dimensional terrain correction in magnetotelluric surveys. *Geophysics*, 1988, **53**, 854–862.
3. Fischer, G., A strong topographic valley effect in AMT and VLF–R measurements. *Geophys. J.*, 1989, **96**, 469–475.
4. Jiracek, G. R., Near-surface and topographic distortions in electromagnetic induction. *Surv. Geophys.*, 1990, **11**, 163–203.
5. Wannamaker, P. E., Stodt, J. A. and Rijo, L., Two-dimensional topographic responses in magnetotelluric models using finite elements. *Geophysics*, 1986, **51**, 2131–2144.
6. Baba, K. and Seama, N., A new technique for the incorporation of seafloor topography in electromagnetic modeling. *Geophys. J. Int.*, 2002, **150**, 392–402.
7. Vozoff, K., The magnetotelluric method. In *Electromagnetic Methods in Applied Geophysics* (ed. Nabighian, M. N.), Society of Exploration Geophysicists, 1991, vol. II, pp. 641–711.
8. Nam, M. J., Kim, H. J., Song, Y., Lee, T. J. and Suh, J. H., Three dimensional topography corrections of magnetotelluric data. *Geophys. J. Int.*, 2008, **174**, 464–474.
9. Ku, C. C., Hsieh, M. S. and Lim, S. H., The topographic effect in electromagnetic fields. *Can. J. Earth Sci.*, 1973, **10**, 645–656.
10. Redding, R. P. and Jiracek, G. R., Topographic modeling and correction in magnetotellurics. In 54th Annual International Meeting, Society of Exploration Geophysicists, Expanded Abstract, 1984, pp. 44–47.
11. Travassos, J. M. and Beamish, D., Distortions of magnetotelluric sounding curves due to a slope. *Geoexploration*, 1988, **25**, 229–244.
12. Li, S., Booker, J. R. and Aprea, C., Inversion of magnetotelluric data in the presence of strong bathymetry/topography. *Geophys. Prospect.*, 2008, **56**, 259–268.
13. Thayer, R. E., Topographic distortion of telluric currents: a simple calculation. *Geophysics*, 1975, **40**, 91–95.
14. Harinarayana, T. and Sharma, S. V. S., Topographic effects on telluric field measurements. *Pageoph*, 1982, **120**, 778–783.
15. Nam, M. J., Kim, H. J., Song, Y., Lee, T. J. and Suh, J. H., Three-dimensional topographic and bathymetric effects on magnetotelluric responses in Jeju Island, Korea. *Geophys. J. Int.*, 2009, **176**, 457–466.
16. Berdichevsky, M. N., Vanyan, L. L. and Dmitriev, V. I., Methods used in the USSR to reduce near-surface inhomogeneity effects on deep magnetotelluric sounding. *Phys. Earth Planet. Inter.*, 1989, **53**, 194–206.
17. Groom, R. W. and Bailey, R. C., Decomposition of magnetotelluric impedance tensors in the presence of local three-dimensional galvanic distortion. *J. Geophys. Res.*, 1989, **94**, 1913–1925.
18. Jiracek, G. R., Redding, R. P. and Kosima, R. K., Application of the Ralyeigh–FFT technique to magnetotelluric modeling and correction. *Phys. Earth Planet. Inter*., 1989, **53**, 365–375.
19. Key, K., Constable, S. and Weiss, C., Mapping 3D salt using 2D marine MT, case study from Gemini Prospect, Gulf of Mexico. In 74th Annual International Meeting, Society of Exploration Geophysicists, Expanded Abstract, 2006, pp. 596–599.
20. Jones, F. W. and Pascoe, L. J., A general computer program to determine the perturbations of alternating electric currents in a two-dimensional model of a region of uniform conductivity with an embedded inhomogeneity. *Geophys. J. R. Astron. Soc*., 1971, **24**, 3–30.
21. Brewitt-Taylor, C. R. and Weaver, J. T., On the finite-difference solution of two-dimensional induction problems. *Geophys. J. R. Astron. Soc*., 1976, **47**, 375–396.
22. Aprea, C., Booker, J. R. and Smith, J. T., The forward problem of electromagnetic induction: accurate finite-difference approximations for two-dimensional discrete boundaries with arbitrary geometry. *Geophys. J. Int.*, 1997, **129**, 29–40.
23. Israil, M., Tyagi, D. K., Gupta, P. K. and Sri Niwas, Magnetotelluric investigations for imaging electrical structure of Garhwal Himalaya corridor, Uttarakhand, India. *J. Earth Syst. Sci*., 2008, **117**, 189–200.
24. Gokarn, S. G., Gupta, G., Rao, C. K. and Selvaraj, C., Electrical structure across the Indus–Tsangpo suture and the Shyok suture zones in NW Himalaya. *Geophys. Res. Lett.*, 2002, **29**, 92.1–92.4.
25. Arora, B. R., Unsworth, M. J. and Rawat, G., Deep resistivity structure of the northwest Indian Himalaya and its tectonic implications. *Geophys. Res. Lett.*, 2007, **34**, L04307.
26. Lemonnier, C. *et al.*, Electrical structure of the Himalaya of central Nepal: high conductivity around the mid crustal ramp along the MHT. *Geophys. Res. Lett.*, 1999, **26**, 3261–3264.
27. Patro, P. K. and Harinarayana, T., Deep geoelectric structure of the Sikkim Himalayas (NE India) using magnetotelluric studies. *Phys. Earth Planet. Inter*., 2009, **173**, 171–176.
28. Gokarn, S. G., Gupta, G., Walia, D., Sanabam, S. S. and Hazarika, N., Deep geoelectric structure over the Lower Brahmaputra valley and Shillong Plateau, NE India using magnetotellurics. *Geophys. J. Int.*, 2008, **173**, 92–104.
29. Rodi, W. and Mackie, R. L., Nonlinear conjugate gradients algorithm for 2-D magnetotelluric inversion. *Geophysics*, 2001, **66**, 174–187.

ACKNOWLEDGEMENTS. We thank the Director, National Geophysical Research Institute, Hyderabad, for permission to publish this work and the Department of Science and Technology, New Delhi, for financial support. We are grateful to the reviewers for their insightful comments.

Received 27 January 2010; revised accepted 11 November 2010